Bismuth Microparticles as Advanced Anodes for Potassium Ion Battery

*Jiaqiang Huang, Xiuyi Lin, Hong Tan, and Biao Zhang**

Dr. J. Huang, Dr. X. Lin, H. Tan, and Dr. B. Zhang
Department of Applied Physics
The Hong Kong Polytechnic University
Hung Hom, Hong Kong
E-mail: biao.ap.zhang@polyu.edu.hk

Keywords: potassium ion batteries, bismuth, anodes, microparticles, phase transitions

Potassium ion batteries (KIBs) are important alternatives to lithium and sodium ion batteries. Herein, microsized Bi electrode delivers exceptional potassium storage capacity, stability, and rate capability by the formation of elastic and adhesive oligomer-containing solid electrolyte interface with the assistance of diglyme electrolytes. The kinetics-controlled K-Bi phase transitions are unraveled combining electrochemical profiles, *in situ* X-ray diffraction and density functional theory calculations. Reversible, stepwise Bi-KBi_2-K_3Bi_2-K_3Bi transitions govern the electrochemical processes after the initial continuous surface potassiation. The Bi electrode outperforms the other anode counterparts considering both capacity and potential. This work provides critical insights into the rational designs of high-performance anode materials for KIBs.

The transition from fossil fuels to renewable energies such as solar powers necessitates large-scale energy storage devices. Batteries, particularly lithium ion batteries (LIBs), have been a

natural choice due to their unprecedented success in consumer electronics and electric vehicles. However, the low content of lithium in the earth crust together with the already demanding market casts doubts on their availability in grid-scale applications.[1, 2] Consequently, sodium and potassium ion batteries have emerged as cost-effective alternatives owing largely to their earth abundance.[1-3] Tremendous efforts have been put into sodium ion batteries (SIBs) during the past several years. Progress on potassium ion batteries (KIBs) was relatively slow due to large K ion radius which discourages the design of promising cathodes. Recent reports on Prussian blue analogues[4] and layered oxides cathodes[5] present competitive energy densities with the counterparts in LIBs and SIBs. The discoveries together with low redox potential of K (-2.93 V vs. -2.70 V for Na) indicate the possibility of building low-cost and high-energy-density KIBs provided that decent anodes are available.[6] It is of great benefit that K ions could be intercalated into graphite. Various carbon materials have been developed as the anodes.[7-9] Nevertheless, the stage I potassium GIC (KC_8) only delivers a modest theoretical capacity of 279 mAh g^{-1}, 75% of that in LIBs (LiC_6).[7] High-capacity alloys such as Sn_4P_3 and Sb have therefore been explored to narrow the apparent gap,[3, 10, 11] in addition to the sulfides.[12, 13] Nonetheless, their fast capacity decay and poor rate capability urgently call for further investigations,[3, 10, 11] since large-radius potassium probably induces the rather huge volume expansion and slow kinetics.

Reducing the size of alloy anodes to nanoscale has been proved effective in suppressing their mechanical fracture.[15] Nanostructured materials also bring about several advantages such as the addition capacities from the pseudocapacitive effect.[16] However, it is inevitably accompanied by unstable solid electrolyte interface (SEI) and large irreversible capacities.[17] In addition, the use of nanomaterials significantly raises the fabrication cost and sacrifices the volumetric energy density, which in turn limit their real applications. Microsized electrodes are therefore highly desired if the volume expansion issue is properly addressed.[18-21] Instead of constructing nanostructures, we turn to engineering the electrolyte-

electrode interphase to constrain the volume expansion in current study. Glyme-based electrolyte has been used in K-ion battery to enable the co-intercalation of solvated K ions into graphite,[22, 23] but their effects in potassium-based alloy anodes remain unknown. It is employed here to build stale SEI on Bi anodes, rendering structural stability of microsized Bi toward long-term cycling. It is also noted that most of alloys theoretically deliver lower capacities in KIBs than the ones in LIBs/SIBs due to the limited potassium intaken before 0 V vs. K/K^+, for example, 369 and 226 mAh g^{-1} for KGe and KSn, respectively.[2] Bismuth has been applied in LIBs,[14] but drawn little attention due possibly to the low gravimetric capacities in comparison to its alloy counterparts such as Si and Sn. In contrast, it stands out as a promising candidate for KIBs in this work, delivering a relatively high theoretical capacity of 385 mAh g^{-1} as well as a low charge voltage.

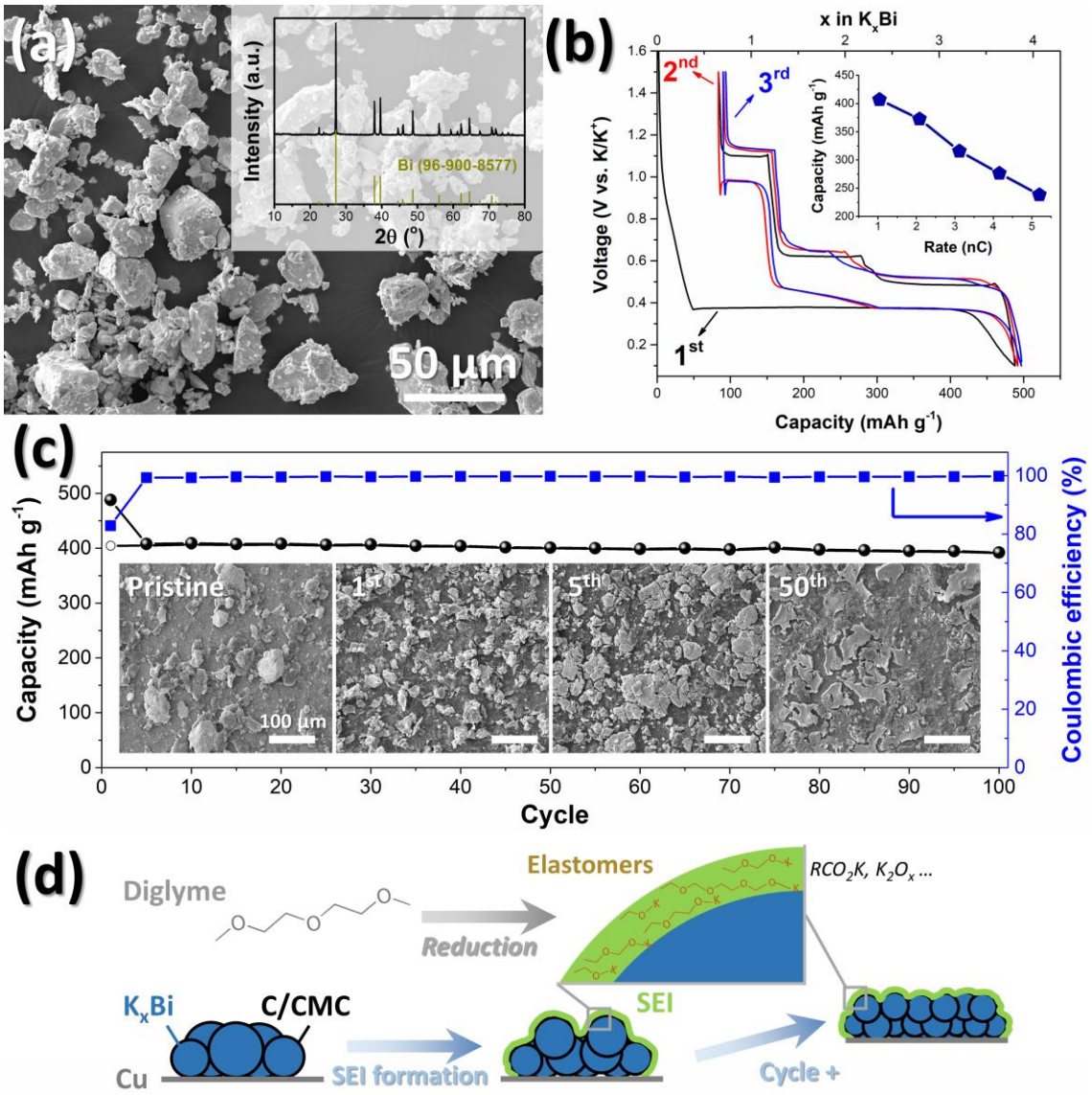

Figure 1. (a) Scanning electron microscopy (SEM) image and the X-ray diffraction (XRD) patterns (inset) of the as-received Bi. (b) Electrochemical curves at 400 mA g^{-1} and the rate capability (inset) of Bi electrode in 1M KPF_6/diglyme electrolyte. (c) Cyclic stability of Bi electrode in 1M KPF_6/diglyme electrolyte at 400 mA g^{-1} and the morphological evolutions after cycles (inset). (d) Schematic illustration of the morphology changes and SEI formation upon electrochemical processes.

The as-received crystalline Bi (200 mesh, **Figure 1**a) was directly used to prepare the electrodes employing carboxymethylcellulose sodium (CMC) as a binder. A mixture of carbon nanofibers and carbon black was used as conductive additives to construct three-dimensional charge transfer channels. Prior to the diglyme electrolyte, carbonate-based

electrolytes, i.e., 1M KPF_6/ethylene carbonate (EC)/propylene carbonate (PC) as used in previous KIBs were adopted.[10, 11] Despite delivering initial capacities of ~400 mAh g^{-1}, the batteries showed low Coulombic efficiencies with large irreversible capacities and fast capacity decay (Figure S1a,b, Supporting Information). These results imply that the instable SEI continuously consumed potassium, decomposed electrolyte and led to the loss of active materials. Fluoroethylene carbonate (FEC) was reported to be a successful stabilizer.[21] A 3 vol.% of FEC was therefore added but only brought about a slight improvement in the cyclic stability (Figure S1c,d, Supporting Information). In sharp contrast, the Bi electrode using 1 M KPF_6/diglyme electrolyte gave a high initial Coulombic efficiency of ~83%, which is the highest value obtained among alloy anodes for KIBs until now. The battery delivered an initial reversible capacity of 404 mAh g^{-1} (Figure 1b). It corresponds that 3.80 potassium ions were involved during the first discharge and 3.15 potassium ions were reversibly extracted during the first charge (Figure 1b). Namely, 0.65 potassium was irreversibly consumed to form the SEI. The reversible value of 3.15 is slightly higher than the theoretical value of 3.0 as discussed later, due to the capacity contributions from carbon (~29 mAh g_{Bi}^{-1} or ~0.23 potassium for Bi, Figure S2, Supporting Information). Remarkably, the Coulombic efficiency readily reached ~98% in the second cycle and remained >99% afterwards. These encouraging results indicate the formation of a stable SEI, who was able to endure the large mechanical strains during the reversible alloying/de-alloying processes. Consequently, the battery delivered a stable capacity up to 392 mAh g^{-1} after 100 cycles, corresponding to a ~97% capacity retention (Figure 1c). The rate capability of the electrode is also superior (Figure 1b, inset). For instance, a capacity of 276 mAh g^{-1} was achieved at a current density of 1600 mA g^{-1} (~4 C). Bi particles of smaller size (~1 μm vs. ~50 μm in diameter) delivered similar electrochemical performance (Figure S3, Supporting Information), showing little size dependence in this range.

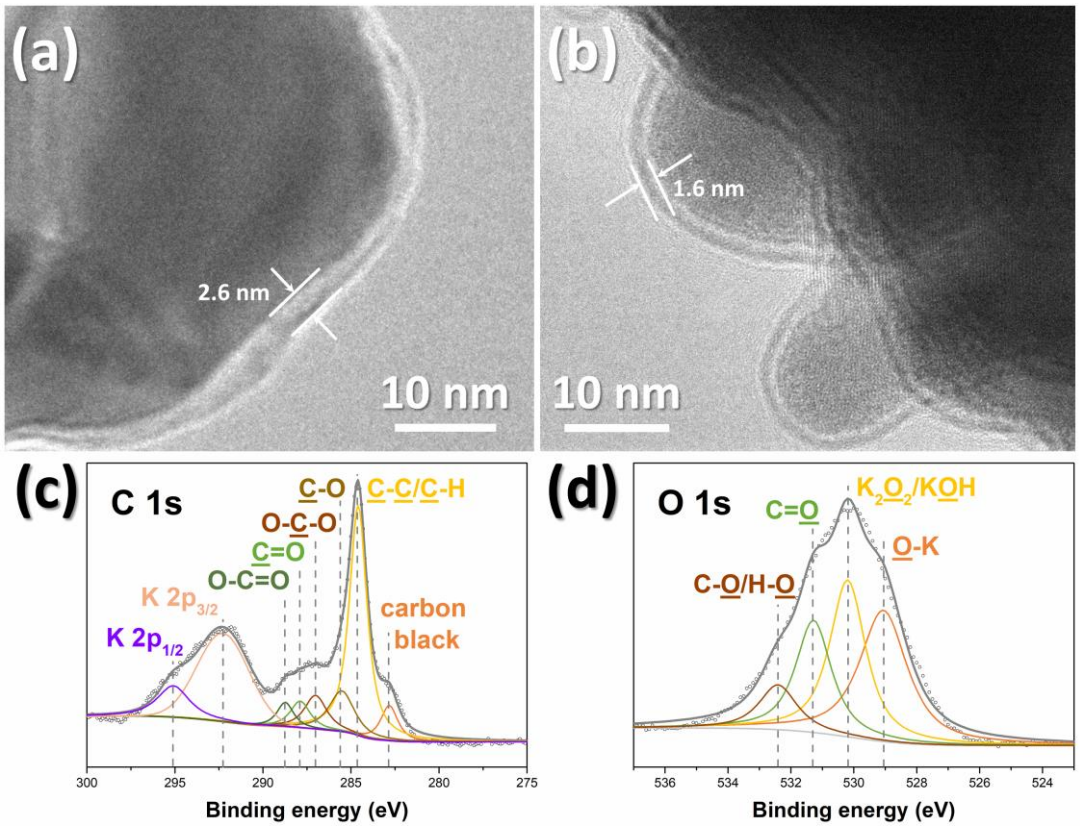

Figure 2. *Ex situ* TEM images of the Bi electrode (a) after cycling and (b) upon the potassiation in 1M KPF_6/diglyme. (c, d) XPS spectra of cycled Bi electrodes in 1M KPF_6/diglyme including (c) C 1s and (d) O 1s.

To examine the mechanism behind the abnormal stability, the morphological evolutions of the electrode are shown in the inset of Figure 1c. Along with the cycle, the original rough surface of the electrode resulting from the Bi microparticles became increasingly smooth. The microparticles were fragmented due to the huge volume change (up to ~406% as discussed later) upon the reversible insertion and extraction of large-radius potassium. However, the continuous and elastic SEI network strongly constrained the particles to avoid their disintegration, as proposed in Figure 1d and seen in Figure 2a,b. The fragments of microparticles (Figure 1c inset) within the SEI did not give rise to many new electrode/electrolyte interfaces, thus leading to the high Coulombic efficiencies after a few cycles.[24] In contrast, The Bi electrodes in carbonate electrolytes suffered from much severe pulverization and visible material isolations after a few cycles (Figure S4, Supporting

Information). The composition of SEI was probed by the energy-dispersive X-ray (EDX) spectroscopy (Figure S5, Supporting Information), which mainly consisted of carbon, oxygen and potassium elements. The X-ray photoelectron spectra (XPS) confirm the formation of C-C(H), C-O, C=O and K-O species (Figure 2c,d). Namely, the SEI consisted of organic and inorganic compounds such as potassium oligomers [$(CH_2CH_2\text{-}O\text{-})_nK$, $(CH_2CH_2\text{-}OCH_2\text{-}O\text{-})_nK$], potassium ethanoate ($RCO_2K$) and K_2O_x. This was further verified by *in situ* Raman spectra with the signatures of oxides and C-O, O=C-O species (Figure S6, Supporting Information). Particularly, these oligomers resulted from structure-similar diglyme, $(CH_3OCH_2CH_2)_2O$, at a minimal cost of reduction, leading to the high initial Coulombic efficiency (Figure 1d). Surprisingly, inorganic K_2CO_3 (XPS and *in situ* Raman) and KF (XPS and EDX) were insignificant in the SEI. On contrary, alkyl carbonates ($ROCO_2K$) were the main components in the EC/PC-derived SEI (Figure S7, Supporting Information). The ether-derived oligomers possessed better mechanical flexibility owing to the elastomeric nature and stronger binding affinity by alkoxy (O-K) edge groups, over the EC/PC-derived counterparts (alkyl carbonates).[25] Therefore, the oligomer-containing SEI uniformly covered the electrode surfaces and was highly tolerant to the huge volume expansion during the K-Bi phase transition (Figure 1d, 2a,b), resulting in the shown superior reversibility.

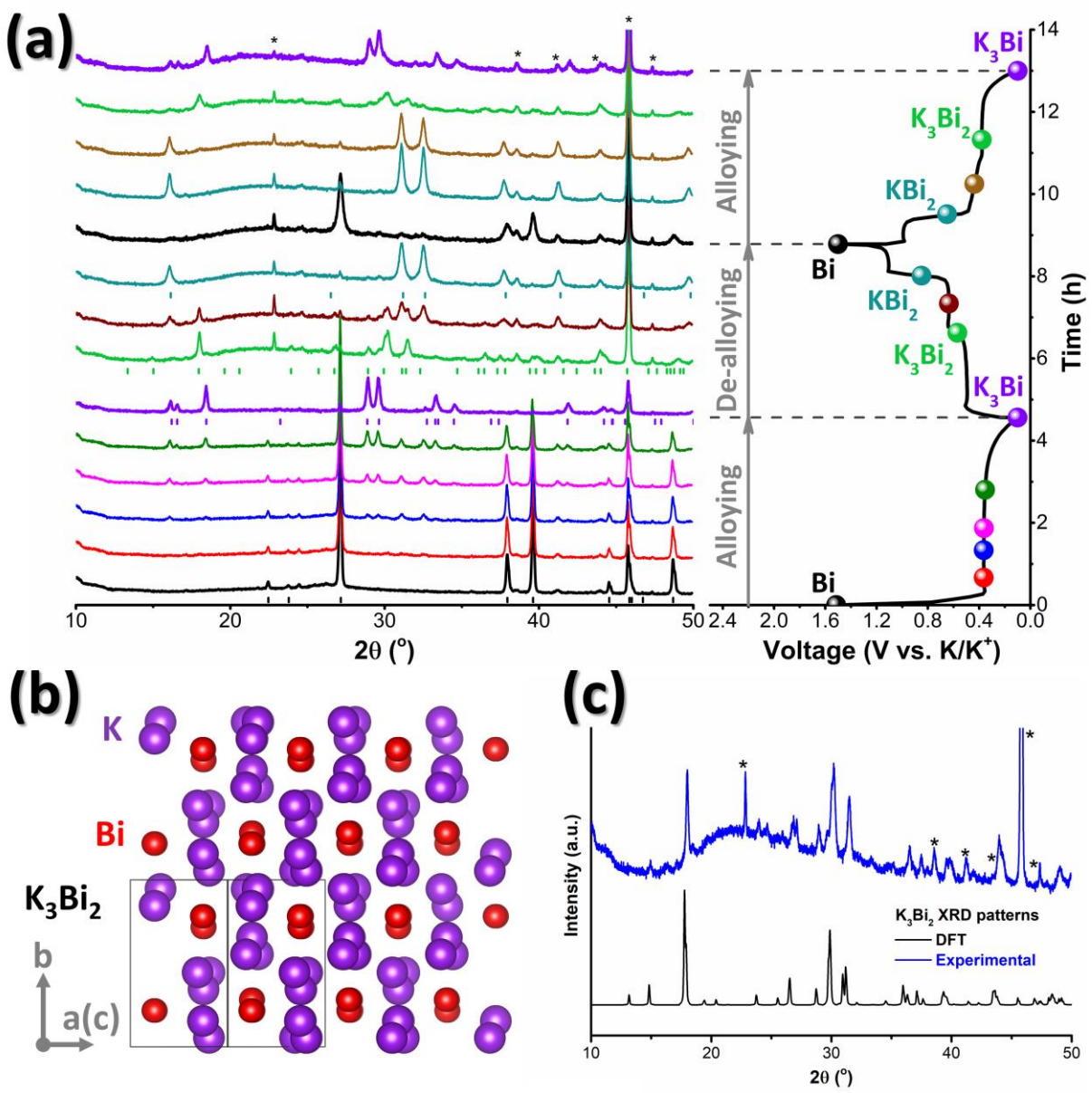

Figure 3. Phase transition of Bi electrode. (a) *In situ* XRD patterns. (b) DFT-calculated crystalline structure of K_3Bi_2 in the monoclinic space group *C2/c*. (c) The simulated XRD patterns in comparison to the experimental one. ~0.2° shift was seen due possibly to the 0 K condition adopted in DFT. The peak at 22.9° is likely associated with K_2O_2, while the other star-labeled peaks come from Be/BeO.

The electrochemical profiles share very similar characteristics in both carbonate- and diglyme-based electrolytes (Figure 1b and S1, Supporting Information), indicating that the alike phase transitions were taking place. Although K-Bi liquid alloys have been investigated in 1980s,[26] the phase transition at room temperature remained largely unknown. To unravel

the potassium storage mechanism in Bi, *in situ* XRD was applied (**Figure 3**a) in conjunction with density functional theory (DFT) calculations. The single plateau of the first discharge profile implies a different phase transition route from the ones in the following cycles (Figure 1b and 3a). The crystalline change was therefore sampled according to the DFT-computed phase diagram (Figure S8, Supporting Information). Cubic KBi_2 and monoclinic K_3Bi_2 were captured when 0.5 potassium was consumed (Figure 3a, red and Figure S9, Supporting Information). In the subsequent potassiation, hexagonal K_3Bi emerged and rapidly grew with the disappearance of K_3Bi_2, while KBi_2 reached a certain intensity and remained almost constant. The co-existence of KBi_2 and K_3Bi and their intensity variations along the plateau suggested a surface potassiation route, where KBi_2 served as the reaction frontier (**Scheme 1**a). At the end of the discharge, K_3Bi became the final phase at the expense of KBi_2 and remaining Bi.

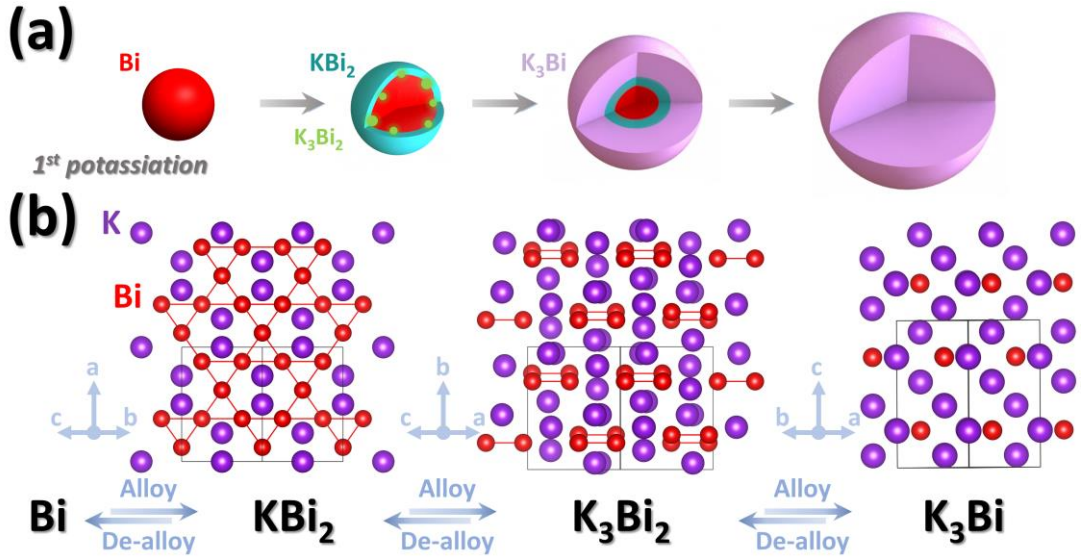

Scheme 1. Alloying and de-alloying processes in Bi electrode in (a) the first discharge and (b) the following cycles.

Unlike the first discharge, the following electrochemical profiles showed a cascade-like characteristic (Figure 1b), suggesting a multi-step phase transition. It was found that the charge plateau at ~0.5 V vs. K/K^+ corresponds to the conversion from K_3Bi to K_3Bi_2. Note that K_3Bi_2 is an absent phase in the existing databases, and was therefore structurally relaxed

by DFT (Figure 3b) on the basis of Cs_3Bi_2 analogue.[27] Good agreements were noted between the theoretical and experimental XRD patterns (Figure 3c). The charge plateaus at ~0.6 and ~1.1 V vs. K/K^+ were identified to be the K_3Bi_2-KBi_2 and KBi_2-Bi transitions, respectively (Figure 3a). The following phase transitions in discharge were entirely reverse to the ones in charge (Figure 3a and Scheme 1b). The above conversions were further supported by the theoretical/experimental electrochemical profiles (**Figure 4**a). Good consistence in both potassium contents and potentials was seen. Without detecting K_5Bi_4 and KBi, this Bi-KBi_2-K_3Bi_2-K_3Bi series transition does not comply with the cases in K-Bi liquid alloy[26] or theoretically predicted phase diagram (Figure S8, Supporting Information). It indicates that the processes are likely controlled by kinetics instead of thermodynamics.

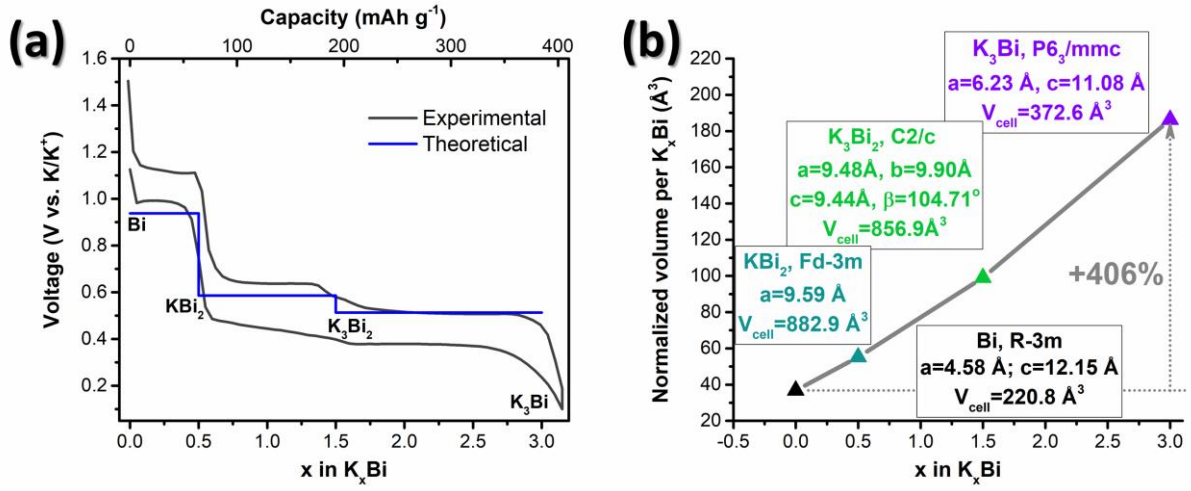

Figure 4. (a) The calculated electrochemical profile in comparison to the second discharge/charge curves. (b) Volume change of the identified K-Bi alloys. The insets show the detailed crystalline parameters computed by DFT.

As summarized in Scheme 1, the Bi electrode took a continuous surface potassiation to form K_3Bi during the first discharge, while the reversible stepwise K_3Bi-K_3Bi_2-KBi_2-Bi de-alloying/alloying mechanisms governed the subsequent cycles. The abundant potassium transfer channels inside the K-Bi crystalline structures (Scheme 1b) benefit the ionic conductivities, while the electrical conductivities are ensured by their (quasi-) metallic nature

as revealed by the density of states (Figure S10, Supporting Information). These results partly explain the superior rate capability of Bi electrodes. A full volume expansion up to ~406% was anticipated from Bi to K_3Bi (Figure 4b), which is nearly twice that of Na_3Bi (~244%) and four times that of Li_3Bi (~106%) (Figure S11, Supporting Information). It highlights the significance of rationally buffering the huge volume expansion in anodes for KIBs, where electrolyte-assisted formation of flexible and good-affinity SEI would be a promising strategy in addition to the electrode morphology engineering.

The average charge voltage is as important as the capacity for the energy density of an anode. The Bi electrode delivered the lowest average charge voltage of 0.65 V vs. K/K^+ among the reported alloy anodes (Table S1, Supporting Information). In addition, the nearly doubled capacities of Bi electrode over the carbon counterparts make the performance outstanding among all the anodes reported (Table S1, Supporting Information). Together with a high capacity retention of ~97% over 100 cycles and the superior rate capabilities, Bi electrode has surely been one of the best KIB anodes up to now (Table S1, Supporting Information). In addition, the tap density of Bi microparticles was measured to be ~5.8 g cm^{-3}, which is nearly six times the one of graphite (~1.0 g cm^{-3})[28]. This in turn gives rise to a siganificant gain of volumetric energy density by using Bi microparticles. To more practically evaluate the anode performance considering both capacity and potential, the energy and power densities of the full batteries were calculated by coupling with $K_xMnFe(CN)_6$ cathode (**Figure 5**).[4] The batteries containing Bi electrode delivered a high energy density of ~312 Wh kg^{-1} and a power density up to ~1506 W kg^{-1}. These values significantly outperform the ones of the other reported anode materials. To test the practical vaule, a full cell was built by coupling Bi anode with a $K_{1.70}Mn[Fe(CN)_6]_{0.90}\cdot 1.10H_2O$ (NI-KMHCF, ~100 mAh g^{-1}) cathode , whichshows a practical energy density of ~251 Wh kg^{-1} and a power density up to ~418 W kg^{-1} (Figure S12, Supporting Information). These values are lower than the estimated ones due mainly to the lower cathode capacities. Noteworthily, KIB can provide a

comparable energy density with the ones of SIBs such as $Na_{3+x}V_2(PO_4)_2F_3/C$ or P'2 $Na_1(Fe_{0.5}Mn_{0.5})O_2/C$.[29] It signifies that KIB is undoubtfully a contender to rival SIB toward sustainable energy storage.

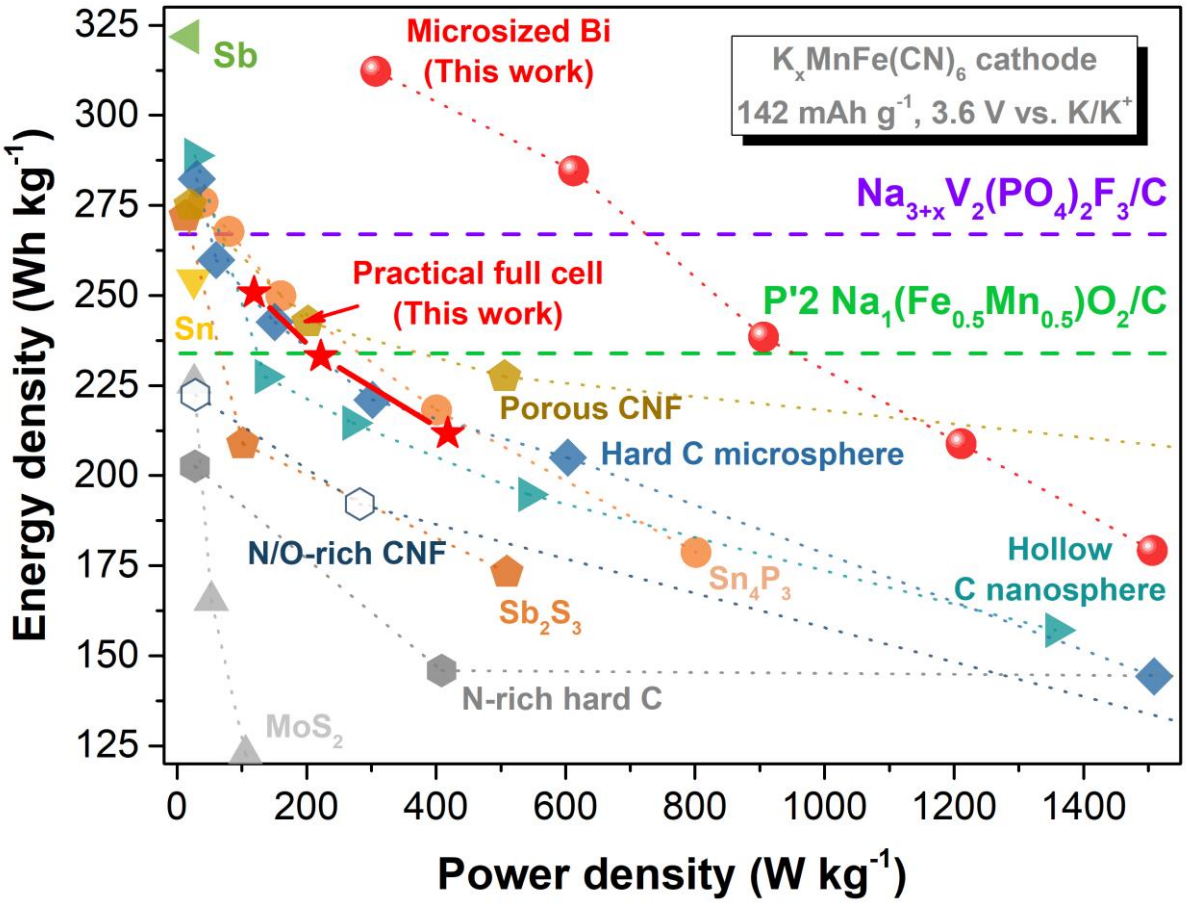

Figure 5. Calculated Ragone plot of the batteries containing the anode materials and a $K_xMnFe(CN)_6$ cathode.[4] The considered KIB anode materials cover alloy-based electrodes including Sn_4P_3,[10] Sb,[11] Sn,[30], sulfide electrodes including MoS_2[12] and Sb_2S_3,[13] and carbon electrodes including hollow C nanosphere,[8], hard C microsphere[9], N-rich hard carbon,[31] porous carbon nanofiber,[32] and N/O-rich carbon nanofiber[33]. The practical full cell data of the batteries containing NI-KMHCF cathode and Bi anode was also plotted. The reference energy densities of $Na_{3+x}V_2(PO_4)_2F_3/C$ and P'2 $Na_1(Fe_{0.5}Mn_{0.5})O_2/C$ are provided.[29]

In summary, Bi microparticle electrode was enabled by forming an elastic oligomer-containing SEI in diglyme electrolytes as a superior anode material for KIBs. The K-Bi phase transitions were unambiguously revealed thanks to the combined electrochemical profiles, *in situ* XRD and DFT calculations. The estimated energy/power densities utilizing the $K_xMnFe(CN)_6$ cathode not only show the notable advantages of Bi electrode over the other anodes but also provide a critical example that proves the potentials of KIBs to compete with SIBs. We anticipate the results shown here will provide profound implications for developing high-performance anode materials for KIBs.

Experimental Section

Preparations of Bi electrode: Commercial Bismuth particles (Macklin, 200 mesh) were adopted as active materials. Bi, carbon nanofiber, super P and CMC were uniformly mixed by mortar and pestle in de-ionized water at a mass ratio of 7:1:1:1. The as-prepared slurry was coated on Cu foil to make a tape. After dried at 60 ^oC overnight, electrodes with a diameter of 12 mm were used for the coin cell assembly. Smaller Bismuth (~1 μm) were purchased from Linker, and the electrodes were prepared in the same way.

Preparations of NI-KMHCF: The material was synthesized according to the literature.[4] The NI-KMHCF was mixed with super P and CMC at a mass ratio of 6:3:1 in de-ionized water, and the slurry was coated on Al foil.

Electrochemical tests: 1M KPF_6 in diglyme, EC/ PC and EC/PC/FEC were prepared as the electrolytes. The volume contents of EC and PC were identical, and the volume ratio of FEC in the EC/PC/FEC electrolyte is 3%. The electrochemical behaviors were captured using coin cells, which were assembled in an Ar-filled glove box. Potassium metal was used as the counter/reference electrode, and the glass fiber (Whatman, GF/D) was utilized as the separator together with a polypropylene membrane (Celgard). The rate capabilities shown in Figure 1b inset were calculated by taking the average of a few measurements. The full cells were assembled with the cycled Bi anode and NI-KMHCF cathode to examine the practical

performance. A Swagelok-type cell was adopted for *in situ* XRD measurements, where the as-prepared slurry was coated on the Be window. These batteries were measured in Arbin and LAND battery systems. *In situ* Raman spectra were acquired using a Swagelok-type cell (EL CELL) on a confocal Raman machine (WITec, alpha 300). The signals shown were collected from the Bi surfaces according to the microscope. The data, particularly the average charge voltage, for the Ragone plot of the other literature was extracted by Engauge Digitizer.[26]

Characterizations: Scanning electron microscope (SEM) images were obtained on Tescan VEGA3. The XRD patterns were collected using the X-ray diffractometer (Rigaku SmartLab) with Cu Kα radiation operating at 45 kV and 200 mA. X-ray photoelectron spectroscopy (XPS, PHI5600, Physical Electronics, Inc.) was carried out using a monochoromatic Al-Kα line at 14 kV. The samples for the *ex situ* SEM and XPS were obtained by disassembling the cells in the glove box, where they were washed with the diglyme or PC/EC, dried in vacuum and sealed in Ar-filled apparatus prior to the observations. *Theoretical calculations:* DFT calculations were carried out applying a projected augmented wave method[27] using generalized gradient approximation parameterized by Perdew-Burke-Ernzerhof[28] performed in the Vienna Ab initio Simulation Package[29]. An energy cutoff of 500 eV was adopted and the k-point was sampled limiting the spacings < 0.05 $Å^{-1}$. The energy and force convergence criteria were 10^{-6} eV and 0.005 eV $Å^{-1}$, respectively. Spin polarization was considered. The equilibrium potentials were calculated according to the following equation.

$$U = \frac{E_{K_xBi} - xE_K - E_{Bi}}{-xe}, \quad (1)$$

where x is the number of electrons involved in the formation reactions, U is the equilibrium potential of the reaction, E_{K_xBi}, E_K and E_{Bi} are the computed total energies of K_xBi, K and Bi at 0 K by DFT, respectively.

Supporting Information

Supporting Information is available from the Wiley Online Library or from the author.

Acknowledgements
This work was financially supported by the Hong Kong Polytechnic University (Grant 1-ZE83) and the Innovation and Technology Commission (ITF Project ITS/029/17) of Hong Kong SAR.

Received: ((will be filled in by the editorial staff))
Revised: ((will be filled in by the editorial staff))
Published online: ((will be filled in by the editorial staff))

References

[1] D. Larcher, J. M. Tarascon, *Nat. Chem.* **2015**, 7, 19.
[2] H. Kim, J. C. Kim, M. Bianchini, D.-H. Seo, J. Rodriguez-Garcia, G. Ceder, *Adv. Energy Mater.* **2017**, 1702384.
[3] I. Sultana, M. M. Rahman, Y. Chen, A. M. Glushenkov, *Adv. Funct. Mater.* **2017**, 1703857.
[4] L. Xue, Y. Li, H. Gao, W. Zhou, X. Lu, W. Kaveevivitchai, A. Manthiram, J. B. Goodenough, *J. Am. Chem. Soc.* **2017**, 139, 2164.
[5] X. Wang, X. Xu, C. Niu, J. Meng, M. Huang, X. Liu, Z. Liu, L. Mai, *Nano Lett.* **2017**, 17, 544.
[6] A. Eftekhari, Z. Jian, X. Ji, *ACS Appl. Mater. Interfaces* **2017**, 9, 4404.
[7] W. Luo, J. Wan, B. Ozdemir, W. Bao, Y. Chen, J. Dai, H. Lin, Y. Xu, F. Gu, V. Barone, L. Hu, *Nano Lett.* **2015**, 15, 7671.
[8] D. S. Bin, Z. X. Chi, Y. Li, K. Zhang, X. Yang, Y. G. Sun, J. Y. Piao, A. M. Cao, L. J. Wan, *J. Am. Chem. Soc.* **2017**, 139, 13492.
[9] Z. Jian, Z. Xing, C. Bommier, Z. Li, X. Ji, *Adv. Energy Mater.* **2016**, 6, 1501874.
[10] W. Zhang, J. Mao, S. Li, Z. Chen, Z. Guo, *J. Am. Chem. Soc.* **2017**, 139, 3316.
[11] W. D. McCulloch, X. Ren, M. Yu, Z. Huang, Y. Wu, *ACS Appl. Mater. Interfaces* **2015**, 7, 26158.
[12] K. Xie, K. Yuan, X. Li, W. Lu, C. Shen, C. Liang, R. Vajtai, P. Ajayan, B. Wei, *Small* **2017**, 13.
[13] Y. Lu, J. Chen, *Sci. China Chem.* **2017**, DOI: 10.1007/s11426.
[14] W. Xianming, T. Nishina, I. Uchida, *J. Power Sources* **2002**, 104, 90.
[15] C. K. Chan, H. Peng, G. Liu, K. McIlwrath, X. F. Zhang, R. A. Huggins, Y. Cui, *Nat. Nanotechnol.* **2008**, 3, 31.
[16] J. Cui, S. Yao, Z. Lu, J.-Q. Huang, W. G. Chong, F. Ciucci, J.-K. Kim, *Adv. Energy Mater.* **2017**, 1702488.
[17] H. Wu, G. Chan, J. W. Choi, I. Ryu, Y. Yao, M. T. McDowell, S. W. Lee, A. Jackson, Y. Yang, L. Hu, Y. Cui, *Nat. Nanotechnol.* **2012**, 7, 310.
[18] B. Zhang, G. Rousse, D. Foix, R. Dugas, D. A. Corte, J. M. Tarascon, *Adv. Mater.* **2016**, 28, 9824.
[19] C. Wang, L. Wang, F. Li, F. Cheng, J. Chen, *Adv. Mater.* **2017**, 29.
[20] S. Choi, T.-w. Kwon, A. Coskun, J. W. Choi, *Science* **2017**, 357, 279.
[21] A. Darwiche, C. Marino, M. T. Sougrati, B. Fraisse, L. Stievano, L. Monconduit, *J. Am. Chem. Soc.* **2012**, 134, 20805.
[22] A. P. Cohn, N. Muralidharan, R. Carter, K. Share, L. Oakes, C. L. Pint, *J. Mater. Chem. A* **2016**, 4, 14954.

[23] H. Kim, K. Lim, G. Yoon, J.-H. Park, K. Ku, H.-D. Lim, Y.-E. Sung, K. Kang, *Adv. Energy Mater.* **2017**, 7, 1700418.
[24] Y. Li, K. Yan, H.-W. Lee, Z. Lu, N. Liu, Y. Cui, *Nat. Energy* **2016**, 1, 15029.
[25] D. Aurbach, *J. Power Sources* **2000**, 89, 206.
[26] A. Petric, A. Pelton, M. Saboungi, *J. Phys. F* **1988**, 18, 1473.
[27] P. Alemany, M. Llunell, E. Canadell, *Inorg. Chem.* **2005**, 44, 1644.
[28] M. Yoshio, H. Wang, K. Fukuda, T. Umeno, T. Abe, Z. Ogumi, *J. Mater. Chem.* **2004**, 14, 1754.
[29] R. Dugas, B. Zhang, P. Rozier, J. M. Tarascon, *J. Electrochem. Soc.* **2016**, 163, A867.
[30] T. Ramireddy, R. Kali, M. K. Jangid, V. Srihari, H. K. Poswal, A. Mukhopadhyay, *J. Electrochem. Soc.* **2017**, 164, A2360.
[31] C. Chen, Z. Wang, B. Zhang, L. Miao, J. Cai, L. Peng, Y. Huang, J. Jiang, Y. Huang, L. Zhang, J. Xie, *Energy Storage Mater.* **2017**, 8, 161.
[32] X. Zhao, P. Xiong, J. Meng, Y. Liang, J. Wang, Y. Xu, *J. Mater. Chem. A* **2017**, 5, 19237.
[33] R. A. Adams, J. M. Syu, Y. Zhao, C. T. Lo, A. Varma, V. G. Pol, *ACS Appl. Mater. Interfaces* **2017**, 9, 17872.